

Charge density gradients of polymer thin film by gaseous phase quaternization

Yeongun Ko¹, Stephanie Christau², Regine von Klitzing³, Jan Genzer^{1,4,*}

¹ Department of Chemical and Biomolecular Engineering, North Carolina State University
Raleigh, NC 27695-7905, USA

² Department of Chemical Engineering, Biointerfaces Institute, University of Michigan
Ann Arbor, MI 48109, USA

³ Department of Physics, Technische Universität Darmstadt
64289 Darmstadt, Germany

⁴ Global Station for Soft Matter, Global Institution for Collaborative Research and Education
Hokkaido University, Sapporo, 060-0808, Japan

Abstract

We report on the rapid formation of charge density gradients in polymer films by exposing poly([2-dimethylaminoethyl] methacrylate) (PDMAEMA) films resting on flat silica substrates to methyl iodide (*i.e.*, MI, also known as iodomethane) vapors. We adjust the charge gradient by varying the MI concentration in solution and the process time. The thickness of the parent PDMAEMA film does not affect the diffusion of MI through and the reaction kinetics in the films. Instead, the diffusion of MI through the gaseous phase constitutes the limiting step in the overall process.

Charged polymers represent an important class of materials, whose chemical and physical properties get tailored by varying, *e.g.*, the distance between charged repeat units or chain topology, leading to variations in diffusion or relaxation dynamics, glass transition, counter ion exchange, and other properties.¹⁻³ Tertiary amines are often employed as parent polymers for post-polymerization modification reactions because they can be tailored to feature zwitterionic, strongly-charged units (after appropriate betanization or quaternization post-polymerization reactions, respectively) or can be weakly-charged in solutions with low pH.⁴⁻⁹

Many researchers have studied the performance of polyelectrolyte thin films due to a

* Corresponding author: jgenzer@ncsu.edu

variety of potential applications, *i.e.*, lubrication, antifouling or antibacterial properties, or cell adhesion, to name a few.^{10–19} Gradients of chemical or physical properties in films enable investigating a given phenomenon of interest in a systematic fashion, thus reducing systematic experimental errors as well as laborious efforts in preparing individual samples while allowing a comprehensive and systematic survey of sample characteristics.^{11,20–23} Substrate-bound material gradients may also act as “engines” that provide a driving force for cell migration or droplet transport.^{24–29} Several research groups prepared charge density gradients and studied their properties. Higgins and coworkers have focused on fabricating charge density gradients using small-molecule organosilanes.^{30–32} Although the gradients were well characterized, the organosilanes possess a few disadvantages, *i.e.*, substrate-dependence, limited chemistry, limited thicknesses, and complex assemblies at interfaces.^{33–35} Lee and coworkers, demonstrated charge density gradients of polymer grafts using corona discharge.^{36,37} Braun and coworkers developed a method to form micrometer-scale gradients of charged polymer brushes by utilizing microfluidics.^{38,39} Very recently, Sun *et al.*⁴⁰ reported on fabricating surface charge density gradients on surfaces by using fluorinated silica nanospheres and using water droplets delivered from different heights above the substrate to form substrate-dependent charge gradients.

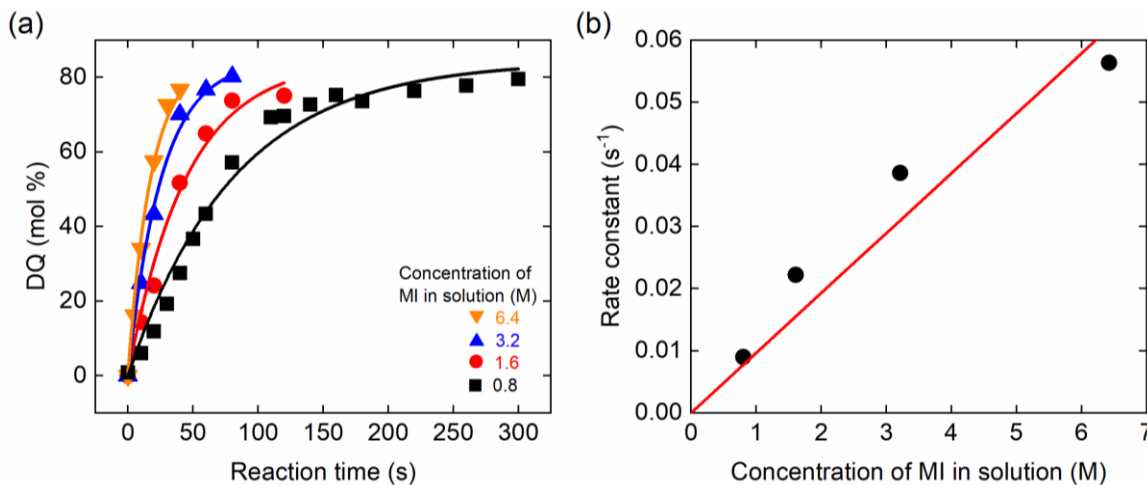


Figure 1. (a) Degree of quaternization (DQ) *vs.* reaction time in ethanol solution with variable methyl iodide (MI) concentration at ambient condition; (b) the rate constant for pseudo-first-order reaction with different MI concentration. The slope, $0.0097 (\text{M} \cdot \text{s})^{-1}$, corresponds to the rate constant of the second-order reaction (k_{2l} , *cf.* **Equation 1**). The dry thickness of the PDMAEMA brushes was $\sim 93 \text{ nm}$ as measured by ellipsometry at 100°C .

Here, we describe a simple method to form charge density gradients in poly([2-dimethylaminoethyl] methacrylate) (PDMAEMA) thin films on flat silica substrates by vapor diffusion of methyl iodide (MI). The process is rapid: at 6.4 M of MI concentration in solution, it takes only \sim 40 seconds to quaternize PDMAEMA films to reach DQ \sim 77 mol%, which is comparable to the maximum DQ obtained in solution (\sim 85 mol%). We form the PDMAEMA layers by either surface-initiated polymerization or deposit PDMAEMA homopolymer films on the substrate by dip-coating (see supporting information, SI, for details). We lower the PDMAEMA-coated wafer vertically into a standard 50 mL beaker (inner diameter 4 cm, height 5.5 cm) and inject MI solution so that the sample contacts barely the solution level. As MI evaporates from the solution, it deposits onto and reacts with the tertiary amines in the DMAEMA units in the films. The latter process forms quaternized (*i.e.*, positively charged) groups in the PDMAEMA films (**Scheme S1**). For each concentration of MI in solution, we adjust the spatial distribution of the charged groups in the substrates by varying the process time (*i.e.*, diffusion of MI in the vapor and through the film and the reaction).

We first studied the quaternization kinetics in the liquid phase by immersing PDMAEMA brush samples into solutions featuring different concentrations in ethanol (*i.e.*, 0.8, 1.6, 3.2, and 6.4 M) for various times. We assumed that the quaternization in the liquid phase is reaction limited given that the diffusion of MI from bulk liquid solution ($D \sim 10^{-5} \text{ cm}^2/\text{sec}$) was very fast even in thick films (\sim 300 nm).^{6,8} We measured the dry thickness of quaternized PDMAEMA (qPDMAEMA) brushes and the degree of quaternization (DQ) using ellipsometry by implementing the method we recently described.⁴¹ The index of refraction of the films increases linearly with increasing DQ.⁴¹ (see SI).

Previously, researchers used a second-order reaction kinetic model to characterize quaternization reactions.^{4,42} Because in our system, MI is present in large excess, we fit the experimental data using pseudo-first-order reaction kinetics (**Equations 1, 2, and Figure 1a**).

$$\frac{dn}{dt} = -k_{2l} \cdot n \cdot c \cong -k_{1l} \cdot n \quad (1)$$

$$\text{DQ (mol \%)} \equiv 100\% \times \frac{n_0 - n}{n_0} = A \times [1 - \exp(-k_{1l} \cdot t)] \quad (2)$$

n_0 , n , c , k_{1l} , k_{2l} , t and A represent the initial concentration of unmodified monomer, the concentrations of unmodified monomer, and MI, respectively, the rate constants for the pseudo-

first-order reaction ($k_{1l} \cong k_{2l} \cdot c$), the second-order reaction in the liquid phase, respectively, the process time, and the upper limit of DQ. The upper limit of DQ was found to be ~ 85 mol% which is in good agreement with the result reported Přádný *et al.* who studied bulk quaternization kinetics of PDMAEMA.⁴ Two major effects may influence the upper limit of quaternization: 1) steric hindrance due to the presence of two bulky methyl groups attached to nitrogen in DMAEMA units,⁴³ 2) decreasing solubility of qPDMAEMA in ethanol with increasing DQ,⁸ accompanied with the associated chain collapse, which limits the reactivity of the remaining unmodified DMAEMA units in the random copolymer with the quaternizing agent.

We fit the experimental data to **Equation 2** and plot the k_{1l} values against different MI solution concentrations in **Figure 1b**, which displays a linear dependence of k_{1l} on the MI concentration in solution (see SI). We then estimate the rate constant for the second-order reaction kinetics, $k_{2l} \sim 0.0097$ (M·s)⁻¹, by using the slope in the linear fit in **Figure 1b**. The obtained value is a little larger than the literature value ~ 0.003 (M·s)⁻¹, measured in bulk reaction.^{4,42} We explain the difference by assuming that our system involves surface reaction, which features highly concentrated reactive centers compared to the bulk polymer solution.⁴⁴ Compared to free polymers in bulk solutions, the swollen brushes exhibit significantly higher local concentration of the reactive repeat units, which accelerates the reaction kinetics.

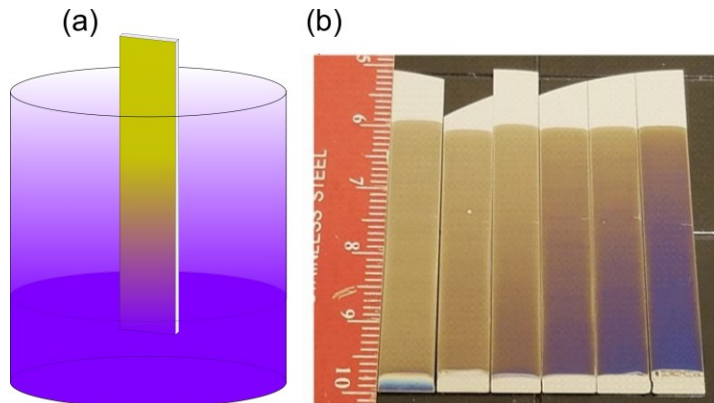


Figure 2. (a) Experimental setup used to produce charge density gradients in polymer films by vapor diffusion of methyl iodide. (b) Quaternized PDMAEMA films formed after exposure to methyl iodide vapors (the units in the ruler are centimeters). The process time was 0 (i.e., just before MI solution injection), 15, 30, 45, 60, and 90 sec from left to right. The concentration of methyl iodide in ethanol solutions was 3.2 M. The dry thickness of the parent PDMAEMA brushes was ~ 70 nm as measured by ellipsometry at 100°C.

We prepared samples featuring charge density gradients of polymer thin films by reacting parent PDMAEMA films with MI vapors (*cf. Figure 2*). Silicon wafers (6 mm \times 40 mm) coated with PDMAEMA films were placed vertically into an empty standard 50 mL glass beaker (inner diameter 4 cm, height 5.5 cm). MI solutions in ethanol (200 μ L) were poured into the beaker so that the bottom portion of the sample (~2-3 mm) was immersed partially in the MI solution. After a given time, the sample was removed from the beaker, dried by flowing nitrogen gas, and the sample refractive index was assessed by ellipsometry. The entire process includes evaporation of MI from solution, diffusion through the air, diffusion through the polymer layer, and reaction with tertiary amines in PDMAEMA. We form charge density gradients in the parent films by using solutions of various MI concentrations and process times.

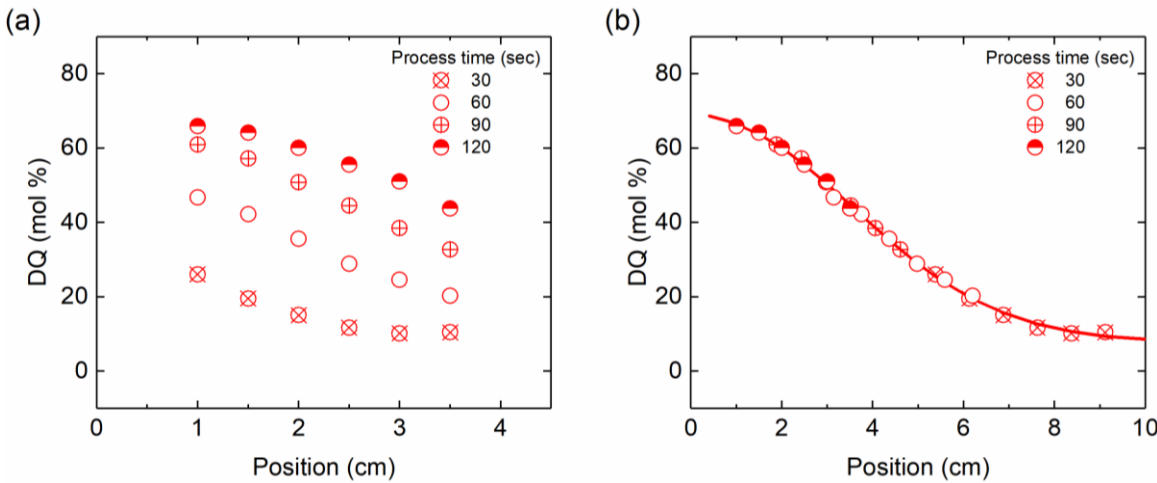


Figure 3. (a) DQ of charge density gradient films with different process time before data shifting. The quaternization in the gaseous phase was achieved with 1.6 M MI in ethanol. (b) The corresponding data after a horizontal shift. The solid curve is the result of fitting the experimental data to **Equation 5** with a constant $D = 0.13 \text{ cm}^2/\text{sec}$ and $t = 120 \text{ sec}$. The shift values are reported in the SI.

We measure the DQ (from the variation of the refractive index at 600 nm) as a function of the position on the sample for various process times. **Figure 3** plots examples of such spatio-temporal profiles for solution concentration of MI in ethanol of 1.6 M. We pick the data set collected at 120 sec as a basis and shift the DQ *vs.* position data in the sample prepared at 90 sec by the same amount along the horizontal axis so that the DQ from both specimens fall onto a master plot. We repeat the same procedure for the remaining data sets. Thus, each data set possesses a unique shift factor. **Figure 4S** in the SI reports shift factors for all samples studied. From the data in **Figure 4a**, which features time shifts from solutions having four different

concentrations of MI in ethanol, we notice that samples prepared by quaternization from solutions having a lower concentration of MI exhibited broader DQ gradients in the films. It indicates that, similar to the reaction in the liquid phase, the MI concentration in vapor influences the kinetics of quaternization. We analyzed the acquired gradient data with the following equations:

$$\frac{dn}{dt} = -k_{2g} \cdot n \cdot c(z, t) \quad (3)$$

$$c(z, t) = c(0, t) \cdot \operatorname{erfc} \left(\frac{z}{2\sqrt{D \cdot t}} \right) \quad (4)$$

$$\text{DQ (mol \%)} = A \times \left\{ 1 - \exp \left\{ -k_{1g} \cdot \left[t \cdot \left(\operatorname{erfc} \left(\frac{z}{2\sqrt{D \cdot t}} \right) - \frac{z \cdot e^{-z^2/4Dt}}{\sqrt{\pi \cdot Dt}} \right) + \frac{z^2 \cdot \operatorname{erfc} \left(\frac{z}{2\sqrt{D \cdot t}} \right)}{2D} \right] \right\} \right\} \quad (5)$$

where z , k_{1g} , k_{2g} , and D are the position, the rate constants for the pseudo-first-order reaction and the second-order reaction in the gaseous phase, and diffusivity, respectively.

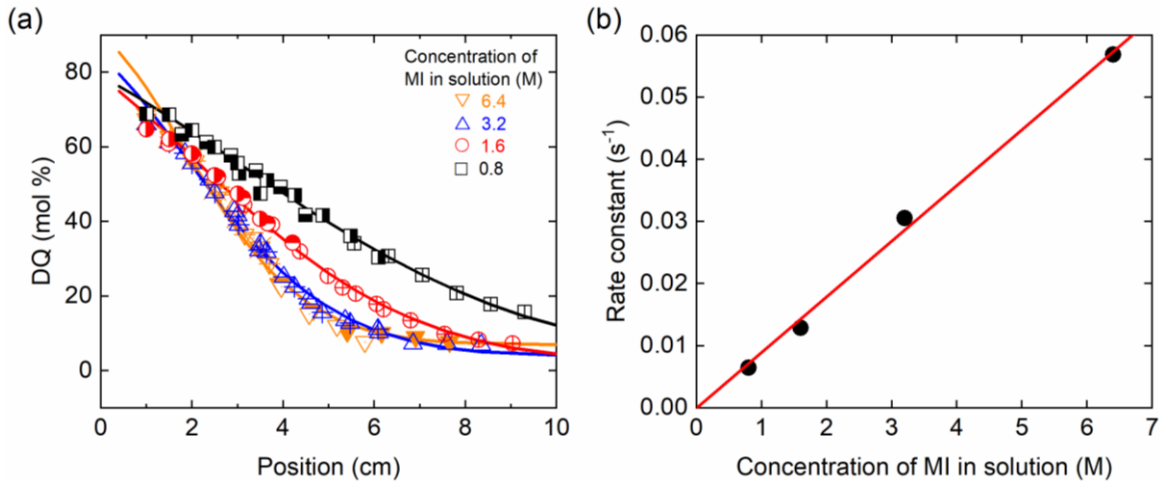


Figure 4. (a) Quaternization gradient with a different nominal concentration of MI in an ethanol solution. The process times for various concentrations are as follows; \times : 10, ∇ : 20, \ddagger : 30, ∇ : 40 sec for 6.4 M, \times : 15, \triangle : 30, \ddagger : 45, \blacktriangle : 60 sec for 3.2 M, \otimes : 30, \circ : 60, \oplus : 90, \bullet : 120 sec for 1.6 M, and \boxtimes : 60, \square : 120, \boxplus : 180, \blacksquare : 240 sec for 0.8 M. Dry thicknesses of PDMAEMA films were \sim 141 nm. The DQ vs. position plots have been obtained by shifting horizontally the data collected at various times (see SI). The symbols represent measured data, and the lines are obtained by fitting the data to **Equation 5**. (b) Rate constants obtained from fitting with different nominal concentrations of MI in solution. The slope is 0.009 $(\text{M} \cdot \text{s})^{-1}$.

Equation 4 allows estimating the MI concentration in the gaseous phase at a certain position and time. The diffusivity of MI in the air is $0.13 \text{ cm}^2/\text{sec}$.⁴⁵ We assume that MI is the excess reagent, and the interfacial concentration of MI, $c(0, t)$, remains constant throughout the process. We solve **Equation 3** and substitute **Equation 4** to obtain **Equation 5**, in which $k_{1g} = k_{2g} * c(0, t)$. We fit all experimental data using **Equation 5** and plot k_{1g} in **Figure 4b** as a function of the concentration of MI in solution. The k_{1g} values are nearly identical to k_{1l} . The k_{1g} changes linearly with the concentration of MI in solution. While we cannot estimate k_{2g} due to the unknown value of $c(0, t)$, we hypothesize that k_{2g} is higher than k_{2l} because the concentration of MI in the gaseous phase should be lower than that in the liquid. In the SI document, we provide evidence that our assumption is correct.

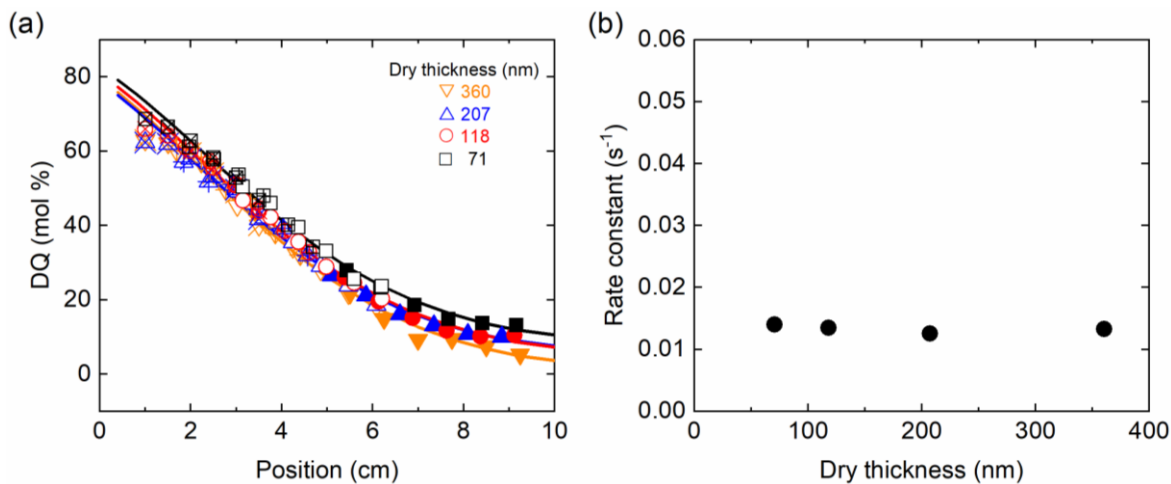


Figure 5. (a) Quaternization gradient with different PDMAEMA film thicknesses. The process times for various thicknesses are following; ∇ : 30, ∇ : 60, ∇ : 90, ∇ : 120 sec for 360 nm, ∇ : 30, Δ : 60, ∇ : 90, Δ : 120 sec for 207 nm, \otimes : 30, \circ : 60, \oplus : 90, \odot : 120 sec for 118 nm, and \boxtimes : 30, \square : 60, \boxplus : 90, \boxdot : 120 sec for 71 nm. All modifications were carried out with 1.6 M of MI in an ethanol solution. The lines are obtained by fitting the data to **Equation 5**. (b) Rate constants obtained from fitting with different dry thicknesses of polymer films.

The diffusion of MI involves two distinguishable processes: 1) transport through the gaseous phase, and 2) diffusion through the polymer layer resting on the substrate. To gain insight into which diffusion process controls the entire kinetics, we repeated the experiments with PDMAEMA films of thicknesses ranging from 71 to 360 nm (**Figure 5**). The results plotted in **Figure 5b** show that all k_{1g} values are the same regardless of the initial thickness of the parent

PDMAEMA film, which implies that the reaction kinetics is not affected by the PDMAEMA thicknesses.

In summary, we examined the quaternization kinetics of PDMAEMA films by MI vapors and modeled them with a pseudo-first-order reaction kinetic model. The reaction kinetics is very fast (*i.e.*, it takes ~40 seconds to achieve DQ ~77 mol%). The thickness of the polymer layer does not affect the diffusion in the studied thickness range or the reaction kinetics. The independency of the film thickness on the entire process implies that vapor transport is the limiting process, similar to vapor deposition of organosilanes onto flat silica substrates.^{46–48} The linearity between the shift factors and the square root of process time (*cf. Figure S4*) supports this claim. We thus suggest that the overall process is governed primarily by methyl iodide diffusion through the gaseous phase. We note that the “steepness” of the gradient depends on the height of the beaker. In the experiments described here, we used a standard 50 mL beaker. Using a shorter beaker one can produce sharper gradients; see SI for details.

A major advantage of this vapor deposition set up (besides its fast kinetics) is that it applies to both grafted and non-grafted polymer films. In the pseudo-first-order category of systems, position-dependent and gradually-varying degree of quaternization in free films offers a sound platform for ion transport studies, combinatorial investigation of optical and thermal (refractive index, glass transition) properties of thin films, and other phenomena. One may use this process in multi-step manufacture of complex combinatorial polymer coatings that feature a directional variation of other properties, *i.e.*, position-dependent grafting density or molecular weight of polymer brushes.

Associated content

Supporting information

The Supporting Information is available free of charge on the ACS Publications website.

Preparation and characterization of polymer films. Temperature sweep of PMMA layers. Film thickness for different polymer solution concentration. Data shifting process (PDF).

Author information

*Email: jgenzer@ncsu.edu

ORCID: Yeongun Ko: 0000-0001-5770-6707

ORCID: Stephanie Christau: 0000-0003-1152-5606

ORCID: Regine von Klitzing: 0000-0003-0555-5104

ORCID: Jan Genzer: 0000-0002-1633-238X

Acknowledgment

The work was supported by the National Science Foundation, Grant no. DMR-1404639 and by the German Research Council (DFG) via the IRTG 1524. We appreciate the partial support from the National Science Foundation, Grant no. DMR-1809453.

References

- (1) Eisenberg, A.; Farb, H.; Cool, L. G. Glass Transitions in Ionic Polymers. *J. Polym. Sci. Part A-2 Polym. Phys.* **1966**, *4*, 855–868.
- (2) Muthukumar, M. 50th Anniversary Perspective: A Perspective on Polyelectrolyte Solutions. *Macromolecules* **2017**, *50*, 9528–9560.
- (3) Polymeropoulos, G.; Zapsas, G.; Ntetsikas, K.; Bilalis, P.; Gnanou, Y.; Hadjichristidis, N. 50th Anniversary Perspective: Polymers with Complex Architectures. *Macromolecules* **2017**, *50*, 1253–1290.
- (4) Přádny, M.; Ševčík, S.; Vlček, P. Precursors of Hydrophilic Polymers. *Polym. Bull.* **1984**, *12*, 337–342.
- (5) Bütün, V.; Armes, S. P.; Billingham, N. C. Selective Quaternization of 2-(Dimethylamino)Ethyl Methacrylate Residues in Tertiary Amine Methacrylate Diblock Copolymers. *Macromolecules* **2001**, *34*, 1148–1159.
- (6) Sanjuan, S.; Perrin, P.; Pantoustier, N.; Tran, Y. Synthesis and Swelling Behavior of PH-Responsive Polybase Brushes. *Langmuir* **2007**, *23*, 5769–5778.
- (7) Cheng, N.; Bao, P.; Evans, S. D.; Leggett, G. J.; Armes, S. P. Facile Formation of Highly Mobile Supported Lipid Bilayers on Surface-Quaternized PH-Responsive Polymer Brushes. *Macromolecules* **2015**, *48*, 3095–3103.
- (8) Galvin, C. J.; Genzer, J. Swelling of Hydrophilic Polymer Brushes by Water and Alcohol Vapors. *Macromolecules* **2016**, *49*, 4316–4329.
- (9) Ko, Y.; Genzer, J. Spontaneous Degrafting of Weak and Strong Polycationic Brushes in Aqueous Buffer Solutions. *Macromolecules* **2019**, *52*, 6192–6200.
- (10) Richert, L.; Lavalle, P.; Vautier, D.; Senger, B.; Stoltz, J.-F.; Schaaf, P.; Voegel, J.-C.; Picart, C. Cell Interactions with Polyelectrolyte Multilayer Films. *Biomacromolecules* **2002**, *3*, 1170–1178.
- (11) Kim, M. S.; Khang, G.; Lee, H. B. Gradient Polymer Surfaces for Biomedical Applications. *Prog. Polym. Sci.* **2008**, *33*, 138–164.
- (12) Gribova, V.; Auzely-Velty, R.; Picart, C. Polyelectrolyte Multilayer Assemblies on Materials Surfaces: From Cell Adhesion to Tissue Engineering. *Chem. Mater.* **2012**, *24*, 854–869.
- (13) Galvin, C. J.; Genzer, J. Applications of Surface-Grafted Macromolecules Derived from Post-Polymerization Modification Reactions. *Prog. Polym. Sci.* **2012**, *37*, 871–906.
- (14) Krishnamoorthy, M.; Hakobyan, S.; Ramstedt, M.; Gautrot, J. E. Surface-Initiated Polymer Brushes in the Biomedical Field: Applications in Membrane Science, Biosensing, Cell Culture, Regenerative Medicine and Antibacterial Coatings. *Chem. Rev.* **2014**, *114*, 10976–11026.
- (15) Mi, L.; Jiang, S. Integrated Antimicrobial and Nonfouling Zwitterionic Polymers. *Angew. Chemie Int. Ed.* **2014**, *53*, 1746–1754.
- (16) Zhang, W.; Zhao, Q.; Yuan, J. Porous Polyelectrolytes: The Interplay of Charge and Pores for New Functionalities. *Angew. Chemie Int. Ed.* **2018**, *57*, 6754–6773.

(17) Li, A.; Ramakrishna, S. N.; Nalam, P. C.; Benetti, E. M.; Spencer, N. D. Stratified Polymer Grafts: Synthesis and Characterization of Layered “Brush” and “Gel” Structures. *Adv. Mater. Interfaces* **2014**, *1*, 1–8.

(18) Séon, L.; Lavalle, P.; Schaaf, P.; Boulmedais, F. Polyelectrolyte Multilayers: A Versatile Tool for Preparing Antimicrobial Coatings. *Langmuir* **2015**, *31*, 12856–12872.

(19) Tomlinson, M. R.; Genzer, J. Formation and Properties of Multivariant Assemblies of Surface-Tethered Diblock and Triblock Copolymers. *Polymer* **2008**, *49*, 4837–4845.

(20) Morgenthaler, S.; Zink, C.; Spencer, N. D. Surface-Chemical and -Morphological Gradients. *Soft Matter* **2008**, *4*, 419–434.

(21) Genzer, J.; Bhat, R. R. Surface-Bound Soft Matter Gradients. *Langmuir* **2008**, *24*, 2294–2317.

(22) Genzer, J. Surface-Bound Gradients for Studies of Soft Materials Behavior. *Annu. Rev. Mater. Res.* **2012**, *42*, 435–468.

(23) Collinson, M. M.; Higgins, D. A. Organosilane Chemical Gradients: Progress, Properties, and Promise. *Langmuir* **2017**, *33*, 13719–13732.

(24) Chaudhury, M. K.; Whitesides, G. M. How to Make Water Run Uphill. *Science* **1992**, *256*, 1539–1541.

(25) Ichimura, K.; Oh, S.-K.; Nakagawa, M. Light-Driven Motion of Liquids on a Photoresponsive Surface. *Science* **2000**, *288*, 1624–1626.

(26) Smith, J. T.; Tomfohr, J. K.; Wells, M. C.; Beebe, T. P.; Kepler, T. B.; Reichert, W. M. Measurement of Cell Migration on Surface-Bound Fibronectin Gradients. *Langmuir* **2004**, *20*, 8279–8286.

(27) Smith, J. T.; Elkin, J. T.; Reichert, W. M. Directed Cell Migration on Fibronectin Gradients: Effect of Gradient Slope. *Exp. Cell Res.* **2006**, *312*, 2424–2432.

(28) Ito, Y.; Heydari, M.; Hashimoto, A.; Konno, T.; Hirasawa, A.; Hori, S.; Kurita, K.; Nakajima, A. The Movement of a Water Droplet on a Gradient Surface Prepared by Photodegradation. *Langmuir* **2007**, *23*, 1845–1850.

(29) Jindan, W.; Zhengwei, M.; Huaping, T.; Lulu, H.; Tanchen, R.; Changyou, G. Gradient Biomaterials and Their Influences on Cell Migration. *Interface Focus* **2012**, *2*, 337–355.

(30) Ashraf, K. M.; Giri, D.; Wynne, K. J.; Higgins, D. A.; Collinson, M. M. Cooperative Effects in Aligned and Opposed Multicomponent Charge Gradients Containing Strongly Acidic, Weakly Acidic, and Basic Functional Groups. *Langmuir* **2016**, *32*, 3836–3847.

(31) Ashraf, K. M.; Khan, M. R. K.; Higgins, D. A.; Collinson, M. M. PH and Surface Charge Switchability on Bifunctional Charge Gradients. *Langmuir* **2018**, *34*, 663–672.

(32) Bautista-Gomez, J.; Forzano, A. V.; Austin, J. M.; Collinson, M. M.; Higgins, D. A. Vapor-Phase Plotting of Organosilane Chemical Gradients. *Langmuir* **2018**, *34*, 9665–9672.

(33) Onclin, S.; Ravoo, B. J.; Reinhoudt, D. N. Engineering Silicon Oxide Surfaces Using Self-Assembled Monolayers. *Angew. Chemie Int. Ed.* **2005**, *44*, 6282–6304.

(34) Steinrück, H.-G.; Schiener, A.; Schindler, T.; Will, J.; Magerl, A.; Konovalov, O.; Li

Destri, G.; Seeck, O. H.; Mezger, M.; Haddad, J.; Deutsch, M.; Checco, A.; Ocko, B. M. Nanoscale Structure of Si/SiO₂/Organics Interfaces. *ACS Nano* **2014**, *8*, 12676–12681.

(35) Steinrück, H.-G.; Will, J.; Magerl, A.; Ocko, B. M. Structure of N-Alkyltrichlorosilane Monolayers on Si(100)/SiO₂. *Langmuir* **2015**, *31*, 11774–11780.

(36) Lee, J. H.; Lee, J. W.; Khang, G.; Lee, H. B. Interaction of Cells on Chargeable Functional Group Gradient Surfaces. *Biomaterials* **1997**, *18*, 351–358.

(37) Lee, J. H.; Khang, G.; Lee, J. W.; Lee, H. B. Platelet Adhesion onto Chargeable Functional Group Gradient Surfaces. *J. Biomed. Mater. Res.* **1998**, *40*, 180–186.

(38) Koo, H.-J.; Waynant, K. V.; Zhang, C.; Braun, P. V. Polymer Brushes Patterned with Micrometer-Scale Chemical Gradients Using Laminar Co-Flow. *ACS Appl. Mater. Interfaces* **2014**, *6*, 14320–14326.

(39) Koo, H.-J.; Waynant, K. V.; Zhang, C.; Haasch, R. T.; Braun, P. V. General Method for Forming Micrometer-Scale Lateral Chemical Gradients in Polymer Brushes. *Chem. Mater.* **2014**, *26*, 2678–2683.

(40) Sun, Q.; Wang, D.; Li, Y.; Zhang, J.; Ye, S.; Cui, J.; Chen, L.; Wang, Z.; Butt, H. J.; Vollmer, D.; Deng, X. Surface Charge Printing for Programmed Droplet Transport. *Nat. Mater.* **2019**, *18*, 936–941.

(41) Ko, Y.; Miles, J. R.; Genzer, J. Determining Water Sorption and Desorption in Thin Hydrophilic Polymer Films by Thermal Treatment. *ACS Appl. Polym. Mater.* **2019**, *1*, 2495–2502.

(42) Přádný, M.; Ševčík, S. Precursors of Hydrophilic Polymers, 5. Activation Parameters of Quaternization of Poly(2-Dimethylaminoethyl Methacrylate) with Methyl Iodide. *Die Makromol. Chemie* **1985**, *186*, 1657–1663.

(43) Hu, G.-H.; Wang, W. A Kinetic Model for Steric Hindrance Effects on Quaternization of Poly(Vinylpyridines). *J. Polym. Sci. Part A Polym. Chem.* **1993**, *31*, 3453–3464.

(44) Brittain, W. J.; Minko, S. A Structural Definition of Polymer Brushes. *J. Polym. Sci. Part A Polym. Chem.* **2007**, *45*, 3505–3512.

(45) Matsunaga, N.; Hori, M.; Nagashima, A. Gaseous Diffusion Coefficients of Methyl Bromide and Methyl Iodide into Air, Nitrogen, and Oxygen. *Heat Transf. Res.* **2009**, *38*, 361–369.

(46) Efimenko, K.; Genzer, J. How to Prepare Tunable Planar Molecular Chemical Gradients. *Adv. Mater.* **2001**, *13*, 1560–1563.

(47) Genzer, J.; Efimenko, K.; Fischer, D. A. Formation Mechanisms and Properties of Semifluorinated Molecular Gradients on Silica Surfaces. *Langmuir* **2006**, *22*, 8532–8541.

(48) Douglas, J. F.; Efimenko, K.; Fischer, D. A.; Phelan, F. R.; Genzer, J. Propagating Waves of Self-Assembly in Organosilane Monolayers. *Proc. Natl. Acad. Sci.* **2007**, *104*, 10324 LP – 10329.

TOC figure

